

Journal of Materials Chemistry C

Accepted Manuscript



This article can be cited before page numbers have been issued, to do this please use: S. Xiang, X. Lv, S. Sun, Q. Zhang, Z. Huang, R. Guo, H. Gu, S. Liu and L. Wang, *J. Mater. Chem. C*, 2018, DOI: 10.1039/C8TC01419A.



This is an Accepted Manuscript, which has been through the Royal Society of Chemistry peer review process and has been accepted for publication.

Accepted Manuscripts are published online shortly after acceptance, before technical editing, formatting and proof reading. Using this free service, authors can make their results available to the community, in citable form, before we publish the edited article. We will replace this Accepted Manuscript with the edited and formatted Advance Article as soon as it is available.

You can find more information about Accepted Manuscripts in the [author guidelines](#).

Please note that technical editing may introduce minor changes to the text and/or graphics, which may alter content. The journal's standard [Terms & Conditions](#) and the ethical guidelines, outlined in our [author and reviewer resource centre](#), still apply. In no event shall the Royal Society of Chemistry be held responsible for any errors or omissions in this Accepted Manuscript or any consequences arising from the use of any information it contains.

To improve efficiency of thermally activated delayed fluorescence OLEDs by controlling the horizontal orientation through optimizing stereoscopic and linear structures of indolocarbazole isomers

Songpo Xiang,^a Xialei Lv,^a Shuaiqiang Sun,^a Qing Zhang,^a Zhi Huang,^a Runda Guo,^a Honggang Gu,^b Shiyuan Liu,^b Lei Wang^{*a}

^a Wuhan National Laboratory for Optoelectronics, Huazhong University of Science and Technology, Wuhan, 430074, P. R. China

^b State Key Laboratory of Digital Manufacturing Equipment and Technology, Huazhong University of Science and Technology, Wuhan, 430074, P.R. China.

*Email: wanglei@mail.hust.edu.cn

Abstract: The molecular structures play a critical role in forming horizontal orientation of the emission transition dipole of light-emitting TADF materials which can improve light outcoupling efficiency of OLEDs. Here, two TADF emitters of **IndCzpTr-1** and **IndCzpTr-2** based indolocarbazole derivatives with the stereoscopic and linear structures were designed and synthesized. With the smaller ΔE_{ST} , better thermal stabilities and preferential horizontal orientation with the orientation order parameter S of -0.264, the green TADF OLED device based **IndCzpTr-2** realized the maximum EQE of 30.0%, maximum current efficiency (CE) of 82.6 cd A⁻¹ without using any optical outcoupling technology, meanwhile the sky-blue TADF OLED with maximum EQE of 14.5% and maximum CE of 28.1 cd A⁻¹ was obtained for **IndCzpTr-1** with homologous device structure.

Introduction

Organic light-emitting diodes (OLEDs) have been flourishing for application in displays and illuminations, recently.¹⁻⁶ The traditional fluorescent emitters show an upper limit internal quantum efficiency(IQE) of 25% due to the fact that only one-quarter of excitons are singlets.^{7, 8} Soon afterwards, the phosphorescent emitters achieving IQE of 100% have been developed for which can harvest both singlet and triplet excitons.^{9, 10} Given the high cost and unclear toxicities of metal complexes of phosphorescent OLEDs, a strategy of the pure organic thermally activated delayed fluorescence (TADF) with 100% theoretical IQE has been proposed by Adachi and co-workers.¹¹⁻¹³ Although the TADF emitters with high external quantum efficiency(EQE) have been reported, there is key bottleneck of theoretic optical outcoupling to realize higher efficiency.¹⁴⁻¹⁶ For achieving superior performance, an efficient strategy is to ameliorate the molecule horizontal orientation. It was possible to achieve EQE of 46% without any external outcoupling technology by optimizing the emitter molecule horizontal orientation in phosphorescent OLEDs.¹⁷ Simultaneously, several molecules with the almost maximum EQE in TADF emitters have been reported according to the strategy.¹⁸⁻²⁶

TADF emitters can convert the triplet excitons to singlet excitons through reverse intersystem crossing (RISC) with a small energy gap (ΔE_{ST}) between the lowest singlet excited state (S_1) and lowest triplet excited state (T_1), while the highest occupied molecular orbital (HOMO) and lowest unoccupied molecular orbital (LUMO) of TADF molecules generally require be separated. Earlier the donor and acceptor were used in

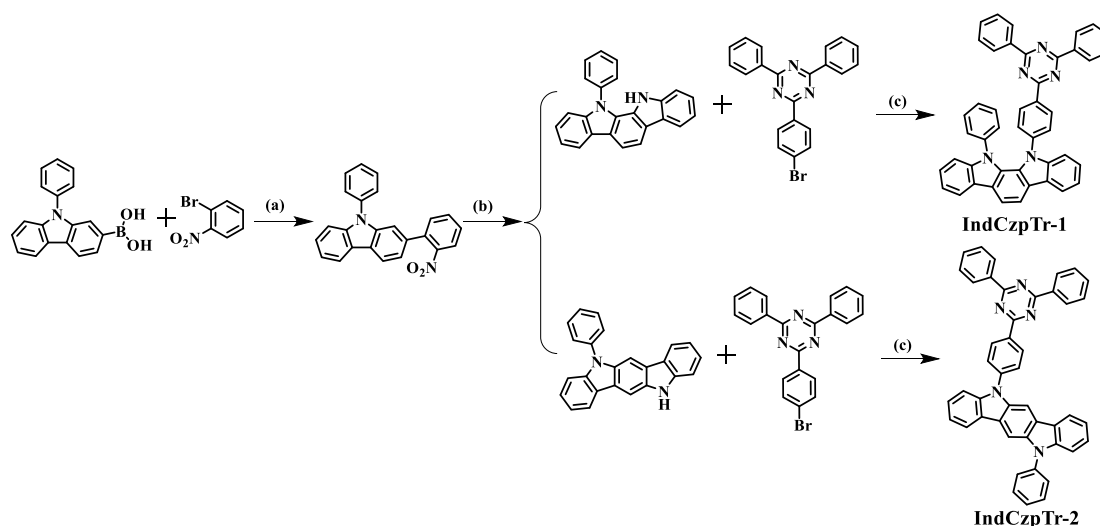
TADF molecule with twisted structures to enhance steric hindrance.²⁷ However, the stereoscopic structure is not beneficial to generate horizontal orientation. On account of that the vertical emitting dipoles in OLEDs generally contribute little to external emission, the radiation pattern of horizontal emitting dipoles is more suitable for optical outcoupling due to the optimal distribution of luminous intensity and suppression of surface plasmon loss.²⁸⁻³¹ Consequently, another designed solution is to stretch distance between planar donor and acceptor moieties, in addition to form more planar and linear molecular structure to improve dipole out-coupling.^{22, 27} The donor and acceptor moieties in TADF molecules both should possess planar structures basing on the designed strategy. In numerous donor moieties, the most of indolocarbazole moieties shows the large planar rigid conjugation structures, and series of indolocarbazole-based TADF materials with superior properties have been reported.³²⁻³⁶ Obviously, the indolocarbazole moieties are potential to constitute planar and linear TADF molecules with superior horizontal orientation by linkage with planar electron acceptor moieties.

According to the designed strategy, two isomeric TADF emitters, 11-(4-(4,6-diphenyl-1,3,5-triazin-2-yl)phenyl)-12-phenyl-11,12-dihydroindolo[2,3-*a*]carbazole (**IndCzpTr-1**) and 5-(4-(4,6-diphenyl-1,3,5-triazin-2-yl)phenyl)-11-phenyl-5,11-dihydroindolo[3,2-*b*]carbazole (**IndCzpTr-2**) based on indolocarbazole donors with different spatial configurations were designed and investigated. The triphenyltriazine moieties were selected as acceptor due to its planar structure, good chemical stability and strong electron-accepting power. With stereoscopic and linear structures, **IndCzpTr-1** and **IndCzpTr-2** endow the different behaviors in photophysical and

electroluminescence properties. Both of materials exhibit excellent thermal stabilities, small ΔE_{ST} , high photoluminescence quantum yield (PLQY) and short decay lifetime. Particularly, the **IndCzpTr-2** shows better horizontal orientation with orientation order parameter (S) of -0.264 from the results of variable angle spectroscopic ellipsometry measurement due to linear structure. The green TADF OLED device based **IndCzpTr-2** realized a high maximum EQE of 30.0% and a maximum current efficiency (CE) of 82.6 cd A^{-1} without using any optical outcoupling technology. Meanwhile the sky-blue TADF OLED with a maximum EQE of 14.5% and a maximum CE of 28.1 cd A^{-1} were obtained for **IndCzpTr-1** with homologous device structure. The results show that TADF OLEDs with higher efficiency could be realized by tuning the molecular structure to improve horizontal orientation.

Results and discussion

Synthesis and Characterization



Scheme 1. Synthetic routes of **IndCzpTr-1** and **IndCzpTr-2**: (a) K_2CO_3 , $\text{Pd}(\text{PPh}_3)_4$, toluene, ethanol, H_2O , 100 °C, 12 h. (b) PPh_3 , 1,2-dichlorobenzene, 180 °C, 24 h. (c) $\text{Pd}(\text{OAc})_2$, $\text{P}(\text{tBu})_3 \cdot \text{HBF}_4$, NaOtBu , toluene, 110 °C, 5 h.

The two target indolocarbazole-based compounds were synthesized by Buchwald-Hartwig coupling reaction and the synthesis route was presented in **Scheme 1**. Besides, the two important intermediate products were obtained from a pot reaction simultaneously as two isomers. Both of the final compounds were purified by vacuum sublimation and the chemical structures were confirmed by nuclear magnetic resonance (NMR) spectroscopy, mass spectroscopy and elemental analysis. The detail synthesis procedures and characterization data are showed in the Experimental Section. Both of the materials exhibit high thermal stabilities, which were estimated via thermogravimetric analysis (TGA) and differential scanning calorimetry (DSC) (as seen in **Fig. S1**). The **IndCzpTr-1** and **IndCzpTr-2** exhibit high decomposition temperatures (T_d) of 426 °C and 448 °C, respectively. Additionally, **IndCzpTr-1** shows a high T_g of 159 °C, while there was no obvious T_g observed for **IndCzpTr-2** from 50 °C to 250 °C. The excellent thermal properties of compounds are beneficial to high-quality film formation and device fabrication through vacuum evaporation.

Table 1. Thermal, Electrochemical, and Photophysical Properties of **IndCzpTr-1** and **IndCzpTr-2**.

Compound	λ_{PL} sol ^a /film ^b (nm)	Φ_{PL} ^c (%)	E_g ^d (eV)	S_1^e/T_1^f (eV)	ΔE_{ST}^g (eV)	τ_p^f (ns)	τ_d^f (μ s)	HOMO/ LUMO ⁱ (eV)	T_g/T_d^j (°C)
IndCzpTr-1	480/492	75.2	2.95	2.94/2.81	0.13	11.09	25.48	-5.47/-2.91	159/426
IndCzpTr-2	490/510	71.9	2.92	2.77/2.66	0.11	8.83	34.31	-5.29/-2.95	no/445

^a Measured in dilute toluene solution at room temperature. ^b Measured neat films at room temperature. ^c Absolute PLQY of these emitters doped in mCBP films with integrating sphere at room temperature. ^d Obtained from the onset of the absorption spectra in toluene solvent. ^e Obtained from the onset of fluorescence spectra in 2-MeTHF at 77K. ^f Obtained from the onset of phosphorescence spectra in 2-MeTHF at 77K. ^g Energy split between S_1 and T_1 estimated from the low temperature fluorescence and phosphorescence spectra. ^h τ_p (the prompt lifetime) and τ_d (the delayed lifetime) were obtained from transient PL decay of doped films. ⁱ HOMO and LUMO energy levels estimated from the redox potential in cyclic voltammetry. ^j T_d obtained from TGA measurements and T_g obtained from DSC measurements.

Theoretical Calculations

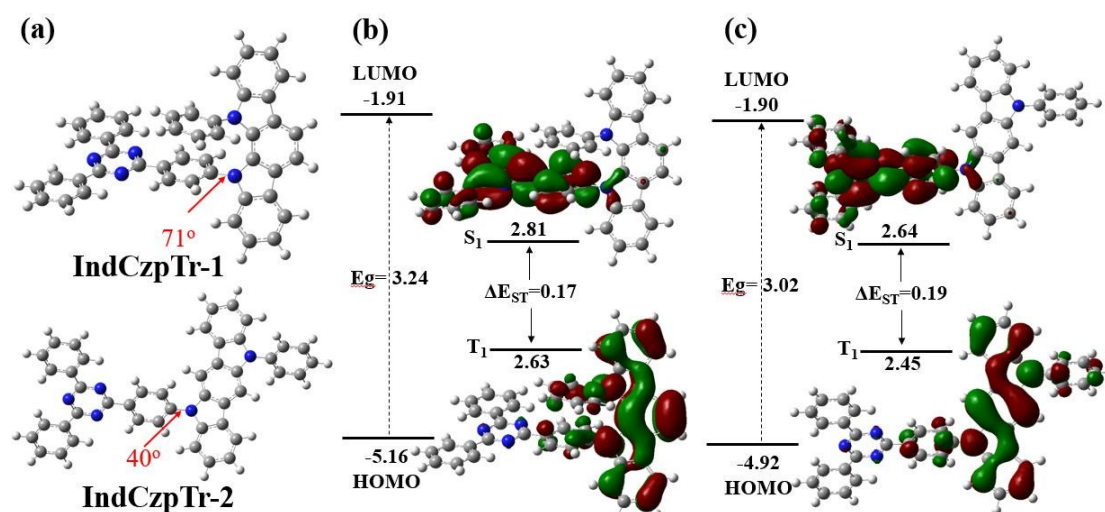
View Article Online
DOI: 10.1039/C8TC01419A

Fig. 1. a) The optimized geometries at the ground state, the HOMO and LUMO distribution of b) **IndCzpTr-1** and c) **IndCzpTr-2**, and the calculated energy levels of compounds.

The molecular configuration and the frontier molecular orbital distribution of **IndCzpTr-1** and **IndCzpTr-2** were analyzed by the density functional theory (DFT) calculations using Gaussian 09 software at the B3LYP/6-31G(d) level. The optimal structures and the distribution of HOMO and LUMO are showed in **Fig. 1**. For two isomeric materials, the different configurations are exhibited. The **IndCzpTr-1** possesses the stereoscopic structure with a twist angle of 71° between **IndCz-1** and triphenyltriazine moieties, while a nearly planar structure is found for **IndCzpTr-2** with a much small twist angle of 40° . For both molecules, the HOMOs are mainly dispersed over the indolocarbazole units, while the LUMOs are fully localized on the triphenyltriazine moiety and the bridging phenyl. The orbital overlap in the bridge phenyl could obviously improve the PLQY of the two compounds as seen in following measurement. In addition, the excited state was calculated using dependent density functional theory (TD-DFT) at the B3LYP/6-31G(d) level to assess the single and triplet excited energies, S_1 and T_1 energies gaps (ΔE_{ST}) and transition dipole moment. As

shown in **Fig. S2**, the HOMO value of **IndCz-2** is shallower than **IndCz-1**, which indicated that **IndCz-2** possesses stronger electron-donating power.³³ Thus, **IndCzpTr-2** exhibits smaller E_g of 3.02 eV, S_1 of 2.64 eV and T_1 of 2.45 eV from calculation, compared with E_g of 3.24 eV, S_1 of 2.81 eV and T_1 of 2.63 eV of **IndCzpTr-1**. Since the similar HOMOs and LUMOs distribution, the similar calculated ΔE_{ST} values of **IndCzpTr-1** and **IndCzpTr-2** are 0.17 eV and 0.19 eV, which potentially enable effective reverse inter-system crossing (RISC) process from T_1 to S_1 .

Electrochemical Properties

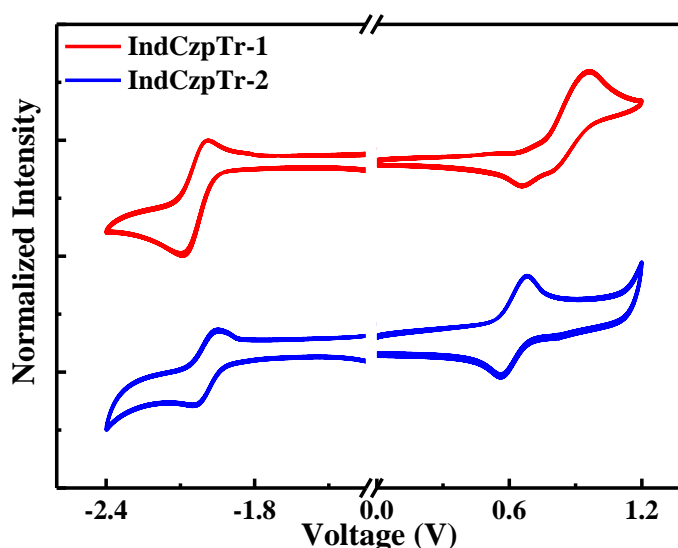


Fig. 2. Cyclic voltammograms of **IndCzpTr-1** and **IndCzpTr-2**.

The electrochemical properties of **IndCzpTr-1** and **IndCzpTr-2** were measured by cyclic voltammetry using traditional three-electrode system. As seen from the **Fig. 2**, the reduction peaks are similar because of the same acceptor of two compounds. Notably, the oxidation potential of **IndCzpTr-2** is lower than that of **IndCzpTr-1**, which demonstrates the stronger electron donating property of the donor in **IndCzpTr-2**. The HOMO and LUMO energy levels were estimated to be -5.47/-2.91 eV for

IndCzpTr-1 and $-5.29/-2.95$ eV for **IndCzpTr-2** with regard to ferrocene. The

View Article Online
DOI: 10.1039/C8TC01419A

experiment results are also in accordance with the trend of calculation consequences.

Photophysical Properties

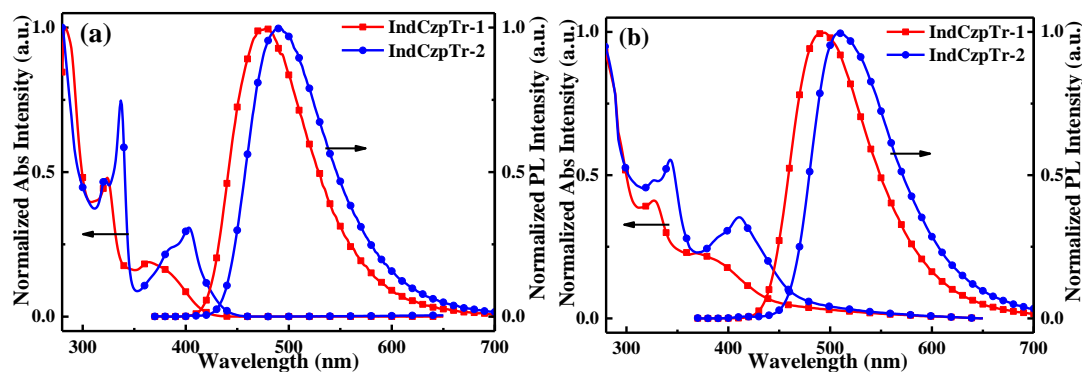


Fig. 3. Absorbance and photoluminescence spectra of **IndCzpTr-1** and **IndCzpTr-2** in a) toluene solvent and b) 20 nm neat films. Emission spectra were excited at 360 nm.

The absorption and photoluminescence (PL) spectra of two compounds were measured in dilute toluene solvents and films, as shown in **Fig. 3**. Two compounds exhibit absorption bands at the range from 300 nm to 350 nm in solvent and film which can be assigned to the indolocarbazole moieties. The ICT absorption bands from the indolocarbazole and triphenyltriazine groups are showed at the around 400 nm. Apparently, the **IndCzpTr-1** shows a slightly blue-shifted absorption because of the more stereoscopic structure leading to reduced conjugation degree. The energy gaps (E_g) of **IndCzpTr-1** and **IndCzpTr-2** which were obtained from the onset of the absorption spectra in toluene solvent are 2.95 eV and 2.92 eV. The peaks in the PL spectra of the **IndCzpTr-1** and **IndCzpTr-2** are found at 480 nm and 490 nm in toluene, 490 nm and 510 nm in film, respectively. The **IndCzpTr-2** exhibits a larger redshift PL, which can be ascribed to the stronger electron-donating ability of **IndCz-2** and the stronger intermolecular reaction. Both of the compounds exhibit similar absorption and

PL spectrum shapes in toluene solvent and films, yet the red-shift between toluene and film indicative of a small increase in electron delocalization in the bulk solid state.³⁷

From the PL of different doped concentrations of **IndCzpTr-1** and **IndCzpTr-2** in mCBP films (**Fig. S3**), no emission is observed from mCBP host, while the photogenerated excitons on hosts smoothly transfer energy to two dopant materials. And with increasing doped concentrations of these films, **IndCzpTr-2** shows the larger red-shifted PL than that of **IndCzpTr-1**, because of the planar structure of **IndCzpTr-2** inducing stronger intermolecular reaction. The PL of two materials in different solvents were tested, and the emissions red-shifted from blue to orange as the polarity of solvent increased, which exhibiting the obvious ICT-state characteristic (**Fig. S4**). The low temperature fluorescence and phosphorescence spectra (**Fig. S5**) in 2-methyltetrahydrofuran (2-MeTHF) solutions were measured to estimate the S_1 energy, T_1 energy and ΔE_{ST} values.³⁸ The S_1 energy levels of **IndCzpTr-1** and **IndCzpTr-2** are 2.94 eV and 2.77 eV, which were obtained from the onset of the low temperature fluorescence. Meanwhile T_1 energy levels are 2.81 eV and 2.66 eV from the onset of the low phosphorescence spectra. As the result, the ΔE_{ST} values were evaluated to be 0.13 eV for **IndCzpTr-1** and 0.11 eV for **IndCzpTr-2**, exhibiting high potential to be TADF materials.

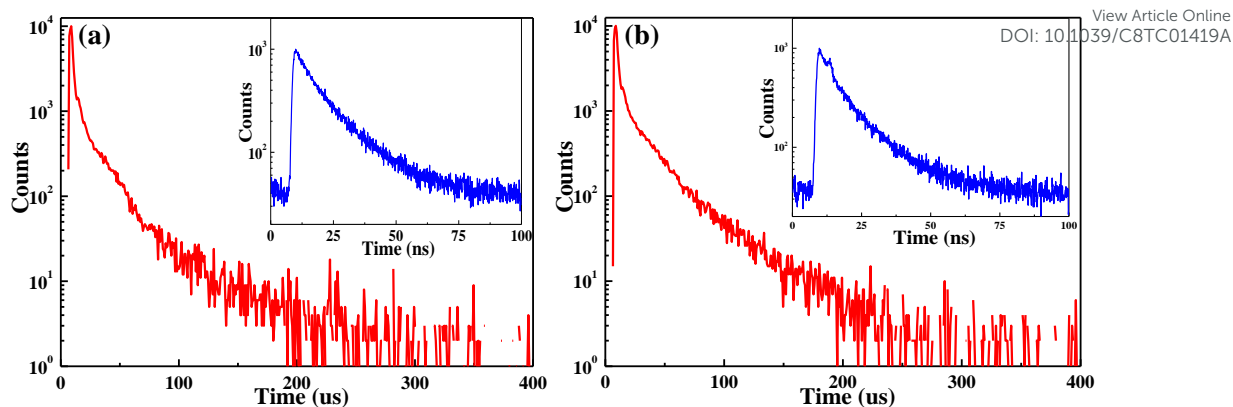


Fig. 4. Transient PL characteristics for delay component of a) **IndCzpTr-1** and b) **IndCzpTr-2** in doped films at 300 K under vacuum. Inset: prompt component of fluorescence decay curve.

In order to confirm the TADF characteristic of **IndCzpTr-1** and **IndCzpTr-2**, the transient PL of doped films were analyzed at room temperature under vacuum. The **Fig. 4** exhibits that **IndCzpTr-1** possesses a prompt emission decay curve from S_1 to S_0 with a lifetime of 11.09 ns and a delayed emission component with a lifetime of 25.48 μ s, and 8.83 ns of prompt component, 34.31 μ s of delay component for **IndCzpTr-2**. The delayed emission should be derived from the thermal up-conversion of energy from T_1 to S_1 , then radiates from S_1 to S_0 . Two materials exhibit similar short delayed lifetimes in the doped films, suggesting the efficient RISC process. The temperature dependent transient PL decay of doped films from 77 K to 300 K was also measured to further confirm the TADF property (**Fig. S6**). The ratio of the delayed emission component gradually increases with the temperature rising, due to the increased T_1 to S_1 up-conversion. Both of materials show high PLQY values of 75.2 % for **IndCzpTr-1** and 71.9 % for **IndCzpTr-2** in doped films, which were measured using an integrating sphere under air atmosphere. Using the PLQY and decay curves, the rate constants were calculated and summarized in **Table S1** according the reported method.³⁹

Molecular orientation

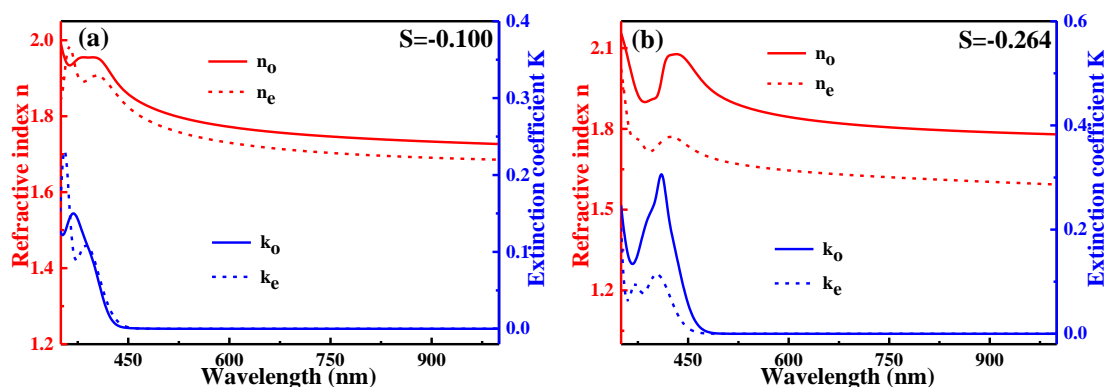


Fig. 5. Ordinary (in-plane) (solid lines) and extraordinary (out-of-plane) (dash lines) refractive indices (n_o , n_e) (red) and extinction coefficients (k_o , k_e) (blue) of neat (non-doped) films of a) **IndCzpTr-1** and b) **IndCzpTr-2**.

Linear structure molecule is potential to realize horizontal orientation, which can increase optical out-coupling efficiency of OLED by the optimal distribution of luminous intensity and suppression of surface plasmon loss. As shown in **Fig. 5**, the orientation order parameter (S) was estimated by variable angle spectroscopic ellipsometry for neat film of **IndCzpTr-1** and **IndCzpTr-2**. By the equation $S = (k_e - k_o) / (k_e + 2k_o)$, where k_o and k_e are the ordinary and extraordinary extinction coefficients at the peak of the band attributed to the transition dipole moment.²⁹ The orientation order parameter S of two materials are -0.1 and -0.264 for **IndCzpTr-1** and **IndCzpTr-2** neat films, respectively. **IndCzpTr-2** exhibits better anisotropy, for which the S is closer to the theoretical value $S = -0.5$ with the perfectly horizontal orientation. And according to value S , the orientation factor (θ) was calculated as the 0.70 for **IndCzpTr-1** and 0.77 for **IndCzpTr-2**.²² The results are derived from the different structures of two materials and the better thermal stability of **IndCzpTr-2**. The preferential horizontal orientation would be formed with significant difference between the deposition temperature ($T_{\text{deposition}}$) and T_g of the film surface.⁴⁰ In the optimized excited

state structures of **IndCzpTr-1** and **IndCzpTr-2**, the transition dipole moments are both along the molecular long axis (**Fig. S7**), however the CT state transition of the longer linear structure of **IndCzpTr-2** is more along the molecular long axis. The calculated results indicate the transition dipole moments of **IndCzpTr-2** directed more along the long molecular axis would enhance the horizontal orientation, matching well with the results of measurement. In addition, the planar structure of **IndCzpTr-2** leads to the strong preferred orientation parallel to the substrate.

Electroluminescent Devices

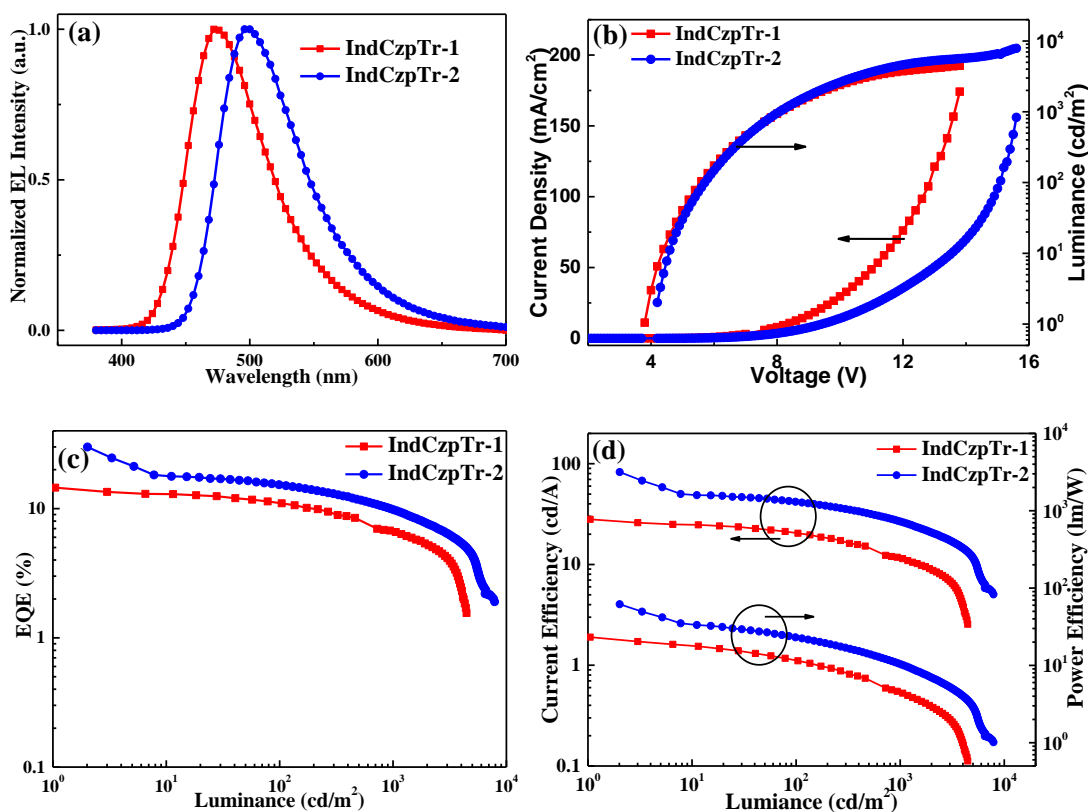


Fig. 6. (a) EL spectra at 100 cd/m². (b) current density–voltage–luminance (J–V–L) characteristics. (c) EQE–luminance characteristics. (d) CE–luminance characteristics and PE–luminance characteristics.

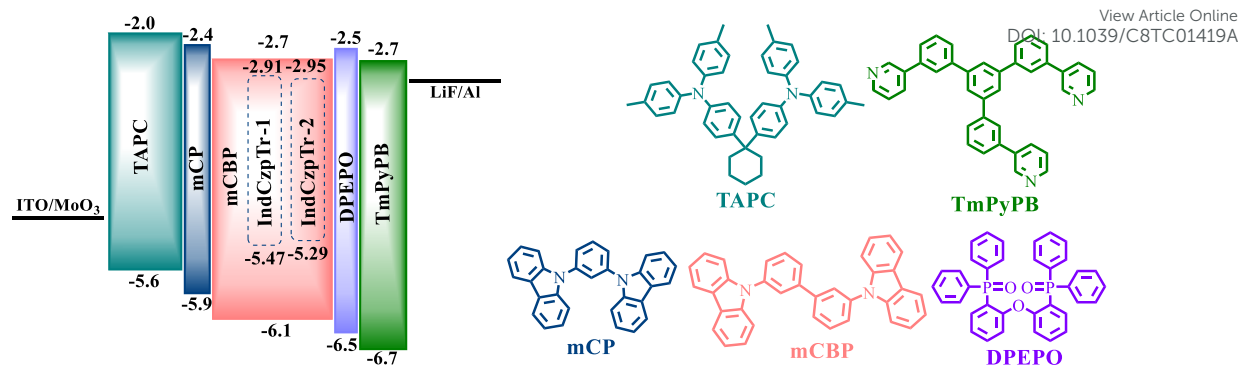


Fig. 7. Energy-level diagram and chemical structures of the materials used in the devices.

Table 2. EL performance of representative TADF OLEDs.

Dopants	V_{on}^a (V)	L_{max}^b (cd m^{-2})	Maximum Efficiency			Efficiency at 100 cd m^{-2}			$\text{CIE}_{(x,y)}$	λ_{EL}^e (nm)
			$\text{EQE}^c(\%)$	$\text{CE}^c(\text{cd A}^{-1})$	$\text{PE}^c(\text{lm W}^{-1})$	$\text{EQE}^d(\%)$	$\text{CE}^d(\text{cd A}^{-1})$	$\text{PE}^d(\text{lm W}^{-1})$		
IndCzpTr-1	3.8	4452	14.5	28.1	23.2	11.0	20.5	11.5	(0.17,0.27)	470
IndCzpTr-2	4.0	7876	30.0	82.6	61.8	15.3	41.9	23.1	(0.23,0.50)	496

^a The maximum luminance. ^b Operating voltages for onset. ^c The maximum efficiencies of EQE (%), CE (cd A^{-1}) and PE (lm W^{-1}). ^d The efficiencies of EQE (%), CE (cd A^{-1}) and PE (lm W^{-1}) at 100 cd m^{-2} . ^e EL peak wavelength.

With the superior properties of **IndCzpTr-1** and **IndCzpTr-2**, multiple electroluminescent devices were fabricated. The EL properties of these devices are showed in **Fig. 6** and summarized in **Table 2**, and the energy level diagram and chemical structures of materials used in the devices is shown in **Fig. 7**. The doped devices were fabricated using the structures of ITO/MoO₃ (10 nm) /TAPC (70 nm) /mCP (10 nm) /EML (20 nm) /DPEPO (5 nm) /TmPyPB (25 nm) /LiF (1 nm) /Al (100 nm), in which ITO (indium tin oxide) was used as the anode, MoO₃ was used as hole injection layer, TAPC (4,4'-(cyclohexane-1,1-diyl)bis(N,N-di-p-tolylaniline)) was used as the hole transporting layer, mCP (N,N-dicarbazoyl-3,5-benzene) was used as an exciton blocking layer, **IndCzpTr-1** and **IndCzpTr-2** doped in mCBP (3,3-di(9H-carbazol-9-yl)) host were used as the emission layer(EML), DPEPO (bis{2-[di(phenyl)phosphino]phenyl}ether oxide) was used as exciton blocking layer,

TmPyPB (1,3,5-tri(m-pyrid-3-yl-phenyl)benzene) was used as the electron transporting layer, LiF was used as electron injecting layer and Al was used as cathode. The doping concentration of emitters was fixed to be 10 wt% for **IndCzpTr-1** and 20 wt% for **IndCzpTr-2** in the EML after optimization of the control device efficiency. As showed in **Fig. 6a**, both EL spectra of sky-blue and green EL demonstrate efficient energy transfer from host to dopant observing for device of **IndCzpTr-1** and **IndCzpTr-2**, respectively. As the results, the device of **IndCzpTr-2** gives maximum external quantum efficiency (EQE) of 30.0 % and current efficiency (CE) of 82.6 cd A⁻¹ without using any optical outcoupling technology which exceed the theoretical value of 25% and a maximum EQE of 14.5 % and maximum CE of 28.1 cd A⁻¹ are obtained for **IndCzpTr-1** with homologous device structure. The high efficiency can be attributed to the high PLQY, small ΔE_{ST} and short delayed lifetime of two materials. Obviously, device of **IndCzpTr-2** exhibits higher external efficiency comparing with that **IndCzpTr-1**. One cause of the results is that the smaller ΔE_{ST} of **IndCzpTr-2** is favorable for utilizing triplet exciton by the fast up-conversion of T₁ to S₁. The major reason is the preferred horizontal dipole orientation of **IndCzpTr-2** with liner structure substantially improving out-coupling efficiency. Meanwhile dopants are apt to improve the horizontally orientation in a host matrix of with random orientation like mCBP.^[6b, 6c] Furthermore, the materials with excellently horizontal dipole orientation trend to possess higher carrier mobility due to the increasing of π - π overlap between adjacent molecules.^[6b, 18] The devices of **IndCzpTr-2** is supposed to possess more balanced carrier if the electrons or holes are trapped and transported by dopants, which would

obviously enhance the efficiency of devices at low brightness. The devices with different concentration of **IndCzpTr-1**, **IndCzpTr-2** in mCBP host were fabricated (**Fig. S8 and Fig. S9**), respectively. With the increasing doping concentration, both emitters exhibit slightly red-shifted EL spectra, which could be ascribed to the stronger interaction between emitter and host under high doping concentration. The detail data of devices was summarized in **Table S2**. Moreover, the theoretical maximum EQE as the orientation factor (θ) by optical simulation was calculated using software setfos. As shown in Fig. S10, the theoretical maximum EQE for device of **IndCzpTr-1** is 14.65527% at $\theta=0.70$, and the theoretical maximum EQE for device of **IndCzpTr-2** is 30.01294% at $\theta=0.77$. The results are matching with the results of experiment.

As shown in **Fig. S11 and Fig. S12**, the hole-only devices and electron-only devices were fabricated with the structure of ITO/MoO₃ (10 nm)/TAPC (70 nm)/mCP (10 nm)/EML (20 nm)/mCP (10 nm)/ TAPC (70 nm)/MoO₃ (10 nm)/Al and ITO/LiF (1 nm)/TmPyPB (25 nm)/DPEPO (5 nm)/EML (20 nm)/DPEPO (5 nm)/TmPyPB (25 nm)/LiF (1 nm)/Al (100 nm). The **IndCzpTr-1** and **IndCzpTr-2** doped in mCBP host with different doping concentration (5 wt%, 10 wt% and 20 wt%) were used as the EML. The results are well-matched with the energy level analysis of device structures. The shallow LUMO cause electrons to be almost trapped into and transported by dopants. However, due to too large energy difference of HOMO between dopants and mCP, the holes will be preferentially injected into host and transported via host then combined with the electrons trapped into by dopants.⁴¹ As discussed above, the trap-assisted mechanism in the OLED devices of **IndCzpTr-2** would realize more balanced

carrier transportation at low brightness to obtain high EQE. Moreover, the efficiency roll-off for both OLED devices at higher brightness may derive from the unbalanced charge carriers and the direct combination of electron and hole on dopants leading to the more intense triplet concentration.

Conclusion

In summary, two TADF emitters of **IndCzpTr-1** and **IndCzpTr-2** based on indolocarbazole derivatives were designed and synthesized. The isomers **IndCz-1** and **IndCz-2** donor moieties were obtained simultaneously from a simple reaction, when combined with triphenyltriazine moieties, the stereoscopic and linear structures were realized. Both of materials possess obvious TADF features with small ΔE_{ST} and moderate delayed lifetimes. Moreover, the **IndCzpTr-2** exhibits smaller ΔE_{ST} , better thermal stabilities and preferential horizontal orientation with the orientation order parameter S of -0.264, the green TADF OLED device based on **IndCzpTr-2** realized the a maximum EQE of 30.0%, a maximum current efficiency (CE) of 82.6 cd A⁻¹ without using any optical outcoupling technology. Meanwhile, the sky-blue TADF OLED with maximum EQE of 14.5 % and maximum CE of 28.1 cd A⁻¹ was obtained for **IndCzpTr-1** with homologous device structure. The results show that TADF OLEDs with higher EQE could be realized by tuning the molecular structure to improve horizontal orientation.

Experimental section

General Methods: The most of experimental conditions and equipment was according to the our reported procedures.⁴² ¹H NMR and ¹³C NMR spectra were

obtained through a Bruker-AF301 AT 400 MHz spectrometer. Mass spectrometry were carried out on a Bruker-Daltonics microflex LT/SH mass spectrometer. Elemental analyses of carbon, hydrogen, and nitrogen were performed on an Elementar (Vario Micro cube) analyzer. TGA was undertaken using a PerkinElmer Instruments (Pyris1 TGA) under the nitrogen environment at a heating rate of $10\text{ }^{\circ}\text{C min}^{-1}$ from 30 to $600\text{ }^{\circ}\text{C}$. The temperature at 5% weight loss was used as the decomposition temperature (T_d). DSC was conducted on a PE Instruments DSC 2920 unit at a heating rate of $20\text{ }^{\circ}\text{C min}^{-1}$ from 50 to $250\text{ }^{\circ}\text{C}$ under a nitrogen atmosphere. The glass transition temperature (T_g) is determined from the second heating scan. Cyclic voltammetry (CV) was carried out on a computer-controlled EG&G Potentiostat/Galvanostat model 283 at room temperature with a conventional three electrode cell, which consisted of a Pt carbon working electrode of 2 mm in diameter, a platinum wire counter electrode, and an Ag/AgNO₃ (0.1 M) reference electrode. The supporting electrolyte was 0.1 M tetra(nbutyl)ammonium hexafluorophosphate ($n\text{Bu}_4\text{NPF}_6$) in CH_2Cl_2 . The onset potential was determined from the intersection of two tangents drawn at the rising and background current of the cyclic voltammogram. All solutions were purged with a nitrogen stream for 10 min before measurement.

UV-Vis absorption spectra were recorded on a Shimadzu UV-VIS-NIR Spectrophotometer (UV-3600). Absolute PLQYs were obtained using a Quantaaurus-QY measurement system (C11347-11, Hamamatsu Photonics). Fluorescence measurements and photoluminescence decay characteristics were carried out using Edinburgh instruments (FLS920 spectrometers). The low temperature fluorescence and

phosphorescent spectra were measured in 2-MeTHF by a spectrofluorimeter (F-4600, Hitachi Inc.) at 77 K cooled by liquid nitrogen.

Molecular orientation in neat films was investigated using an ellipsometry technique. The 100 nm thick films for these measurements were prepared by thermal evaporation on top of precleaned bare silicon substrates. The optical constants of the films were then measured using a variable angle spectroscopic Mueller matrix ellipsometer^{43, 44} (ME-L, Wuhan Eoptics Technology Co., Ltd) at several incident angles varying from 60° to 70° by steps of 5°. The ellipsometry data were then analyzed using an analytical software (Eometrics, Wuhan Eoptics Technology Co., Ltd) to determine the anisotropic extinction coefficients and refractive indices of the films.

Synthesis

Synthesis of 2-(2-nitrophenyl)-9-phenyl-9H-carbazole: A mixture of (9-phenyl-9H-carbazol-2-yl)boronic acid (10 g, 34.84 mmol), 1-bromo-2-nitrobenzene (7.74 g, 38.32 mmol), 50 mL of K₂CO₃ (2 mol/L), toluene (100 mL) and ethanol (50 mL) was added into a three-neck round bottom flask. After bubbling through nitrogen for 15 min, added Pd(PPh₃)₄ (0.4 g, 0.34 mmol) into the solution and heated to 100 °C stirring for 12 h under a nitrogen atmosphere. The solution was cooled to room temperature, extracted with dichloromethane, and dried over anhydrous MgSO₄. After removal of the solvent under reduced pressure, the final residue was purified by column chromatography on silica gel to afford a yellow product (11.0 g, yield 87%). ¹H NMR (400 MHz, CDCl₃) δ [ppm]: 8.10-8.13 (t, *J* = 7.6 Hz, 2H), 7.77-7.79 (d, *J* = 8.0 Hz, 1H),

7.52-7.57 (m, 5H), 7.37-7.46 (m, 5H), 7.31 (s, 1H), 7.23-7.29 (m, 1H), 7.17-7.20 (m, 1H). MS (APCI): calcd for C₂₄H₁₆N₂O₂: 364.1212; found: 364.7592 [M+H]⁺.

Synthesis of 11-phenyl-11,12-dihydroindolo[2,3-*a*]carbazole and 5-phenyl-5,11-dihydroindolo[3,2-*b*]carbazole: (2-nitrophenyl)-9-phenyl-9*H*-carbazole (5 g, 14.75 mmol) and triphenylphosphine (9.67 g, 36.87 mmol) were added into a three-neck round bottom flask. Then the mixture was dried in vacuum and the flask was filled with nitrogen gas, and 150 mL of 1,2-dichlorobenzene was added to dissolve the mixture and heated to 180 °C for 24 hours in a nitrogen atmosphere. After removing the solvent with vacuum distillation, the crude product was purified using column chromatography and two isomers 11-phenyl-11,12-dihydroindolo[2,3-*a*]carbazole and 5-phenyl-5,11-dihydroindolo[3,2-*b*]carbazole were afforded (total yield 63%). 11-phenyl-11,12-dihydroindolo[2,3-*a*]carbazole: ¹H NMR (400 MHz, DMSO) δ [ppm]: 9.78 (s, 1H); 8.26-8.28 (d, *J* = 7.6 Hz, 1H), 8.15-8.17 (d, *J* = 8.0 Hz, 1H), 8.05-8.09 (t, *J* = 8.8 Hz, 2H), 7.73-7.77 (t, *J* = 8.0 Hz, 2H), 7.63-7.67 (t, *J* = 8.0 Hz, 3H), 7.54-7.56 (d, *J* = 8.0 Hz, 1H), 7.29-7.41 (m, 4H), 7.16-7.20 (t, *J* = 7.6 Hz, 1H). MS (APCI): calcd for C₂₄H₁₆N₂: 332.1313; found: 332.7628. [M+H]⁺. **5-phenyl-5,11-dihydroindolo[3,2-*b*]carbazole:** ¹H NMR (400 MHz, DMSO) δ [ppm]: 11.19 (s, 1H), 8.33-8.35 (d, *J* = 7.6 Hz, 1H), 8.25 (s, 1H), 8.14-8.16 (d, *J* = 8.0 Hz, 1H), 8.05 (s, 1H), 7.72-7.75 (m, 4H), 7.54-7.57 (t, *J* = 5.6 Hz, 1H), 7.35-7.48 (m, 4H), 7.24-7.28 (t, *J* = 7.2 Hz, 1H), 7.07-7.11 (t, *J* = 7.2 Hz, 1H). MS (APCI): calcd for C₂₄H₁₆N₂: 332.1313; found: 332.6931.

Synthesis of 11-(4-(4,6-diphenyl-1,3,5-triazin-2-yl)phenyl)-12-phenyl-11,12-dihydroindolo[2,3-*a*]carbazole (IndCzpTr-1): A mixture of 11-phenyl-11,12-

dihydroindolo[2,3-*a*]carbazole (2 g, 6 mmol), 2-(4-bromophenyl)-4,6-diphenyl-1,3,5-triazine (2.32 g, 6 mmol), Pd(OAc)₂ (0.027 g, 0.12 mmol), *tri-tert*-butylphosphine tetrafluoroborate (0.104 g, 0.36 mmol) and NaOtBu (1.44 g, 15 mmol) was added into a 100 mL round bottom flask with nitrogen gas blowing. Dry toluene (50 mL) was added to dissolve the mixture and refluxed for 5 hours in nitrogen atmosphere. Upon cooling, removed the toluene and extracted with dichloromethane, then removed the solvent under vacuum to give the crude product. The crude product was purified with column chromatography, then recrystallized with dichloromethane/hexane to afford light yellow powder (1.9 g, yield: 50 %). ¹H NMR (400 MHz, CDCl₃) δ [ppm]: 8.72-8.74 (d, *J* = 6.4 Hz, 4H), 8.43-8.45 (d, *J* = 8.4 Hz, 2H), 8.05-8.14 (m, 4H), 7.50-7.58 (m, 6H), 7.16-7.33 (m, 6H), 7.05-7.09 (t, *J* = 7.6 Hz, 1H), 6.90-6.98 (m, 4H), 6.75-6.77 (d, *J* = 7.6 Hz, 2H). ¹³C NMR (100 MHz, CDCl₃) δ [ppm]: 171.72, 171.12, 143.99, 143.49, 142.94, 139.98, 136.26, 133.80, 132.62, 129.68, 129.02, 128.89, 128.72, 128.18, 127.80, 126.59, 126.37, 126.31, 125.77, 125.70, 125.36, 125.13, 121.37, 121.11, 120.03, 119.92, 114.15, 113.71, 111.01, 110.90. MS (APCI): calcd for C₄₅H₂₉N₅: 639.2423; found: 639.2841 [M+H]⁺; Elemental analysis (%): calcd for C₄₅H₂₉N₅: C, 84.48; H, 4.57; N, 10.95; found: C 84.77, H 4.44, N 10.79.

Synthesis of 5-(4-(4,6-diphenyl-1,3,5-triazin-2-yl)phenyl)-11-phenyl-5,11-dihydroindolo[3,2-*b*]carbazole (IndCzpTr-2): The synthesis process was referred to the detailed method of **IndCzpTr-1** (yellow powder, yield: 73%). ¹H NMR (400 MHz, CDCl₃) δ [ppm]: 9.09-9.11 (d, *J* = 5.6 Hz, 2H), 8.84-8.86 (d, *J* = 5.6 Hz, 4H), 8.28 (s, 1H), 8.13-8.17 (t, *J* = 7.6 Hz, 2H), 8.09 (s, 1H), 7.95-7.97 (d, *J* = 8.4 Hz, 2H), 7.59-

7.70 (m, 12H), 7.52-7.54 (t, $J = 4.0$ Hz, 1H), 7.42-7.46 (m, 3H), 7.25-7.30 (m, 1H). ^{13}C NMR (100 MHz, CDCl_3) δ [ppm]: 171.84, 171.04, 142.33, 142.12, 141.53, 138.28, 137.35, 136.50, 136.20, 134.70, 132.66, 130.79, 130.05, 129.05, 128.73, 127.38, 127.32, 126.78, 126.23, 126.14, 124.00, 123.76, 123.51, 123.44, 120.41, 120.31, 119.93, 119.48, 109.71, 109.56, 100.13, 100.01. MS (APCI): calcd for $\text{C}_{45}\text{H}_{29}\text{N}_5$: 639.2423; found: 639.2658 $[\text{M}+\text{H}]^+$; Elemental analysis (%): calcd for $\text{C}_{45}\text{H}_{29}\text{N}_5$: C, 84.48; H, 4.57; N, 10.95; found: C 84.74, H 4.47, N 10.79.

Computational details: The geometrical and electronic properties were computed using the Gaussian 09 program package. The ground-state geometry was optimized using density functional theory (DFT) with B3LYP hybrid functional at the basis set level of 6-31G(d). The singlet and triplet states were calculated by time-dependent density functional theory (TD-DFT) with the B3LYP functional at the same basis set level. Molecular orbitals were visualized using Gauss view 5.0 program.

Device fabrication and measurement: Indium tin oxide (ITO) with a sheet resistance of $15 \Omega \text{ square}^{-1}$ was used as the substrate. Prior to use, the ITO glass substrates were pre-cleaned carefully and treated by oxygen plasma for 5 min before device fabrication. Then the sample was transferred to the deposition system. All organic layers and MoO_3 were deposited at a rate of 1 \AA s^{-1} , and subsequently LiF was deposited at 0.2 \AA s^{-1} and then capped with Al (ca. 4 \AA s^{-1}) through a shadow mask in the vacuum of 2×10^{-6} Torr. For all of the OLEDs, the emitting areas were determined by the overlap of two electrodes as 0.09 cm^2 . The EL spectra, CIE coordinates and J-V-L curves of the devices were measured with a PHOTO RESEARCH SpectraScan PR

655 photometer and a KEITHLEY 2400 SourceMeter constant current source. The EQE values were calculated according to previously reported methods. All measurements were carried out at room temperature under ambient conditions.

Acknowledgements

This research work was supported by the NSFC/China (51573065, 51727809), China Postdoctoral Science Foundation(2017M620321), the science and technology support program of Hubei Province (2015BAA075) and the Analytical and Testing Centre at Huazhong University of Science and Technology.

View Article Online
DOI: 10.1039/C8TC01419A

References

1. Z. Yang, Z. Mao, Z. Xie, Y. Zhang, S. Liu, J. Zhao, J. Xu, Z. Chi and M. P. Aldred, *Chem. Soc. Rev.*, 2017, **46**, 915-1016.
2. Y. Im, S. Y. Byun, J. H. Kim, D. R. Lee, C. S. Oh, K. S. Yook and J. Y. Lee, *Adv. Funct. Mater.*, 2017, **27**, 1603007.
3. J. Huang, H. Nie, J. Zeng, Z. Zhuang, S. Gan, Y. Cai, J. Guo, S. J. Su, Z. Zhao and B. Z. Tang, *Angew. Chem. Int. Ed.*, 2017, **56**, 12971-12976.
4. M.-F. Lin, L. Wang, W.-K. Wong, K.-W. Cheah, H.-L. TAM, M.-T. Lee, M.-H. Ho and C. H. Chen, *Appl. Phys. Lett.*, 2007, **91**, 073517.
5. F. Zhao, Y. Wei, H. Xu, D. Chen, T. Ahamad, S. Alshehri, Q. Pei and D. Ma, *Mater. Horiz.*, 2017, **4**, 641-648.
6. K. Tuong Ly, R.-W. Chen-Cheng, H.-W. Lin, Y.-J. Shiau, S.-H. Liu, P.-T. Chou, C.-S. Tsao, Y.-C. Huang and Y. Chi, *Nat. Photon.*, 2016, **11**, 63.
7. M. A. Baldo, D. F. O'Brien, M. E. Thompson and S. R. Forrest, *Phys. Rev. B*, 1999, **60**, 14422-14428.
8. M. Segal, M. A. Baldo, R. J. Holmes, S. R. Forrest and Z. G. Soos, *Phys. Rev. B*, 2003, **68**, 075211.
9. M. A. Baldo, D. F. O'Brien, Y. You, A. Shoustikov, S. Sibley, M. E. Thompson and S. R. Forrest, *Nature*, 1998, **395**, 151.
10. J. S. Wilson, A. S. Dhoot, A. J. A. B. Seeley, M. S. Khan, A. Köhler and R. H. Friend, *Nature*, 2001, **413**, 828.
11. Q. Zhang, B. Li, S. Huang, H. Nomura, H. Tanaka and C. Adachi, *Nat. Photon.*, 2014, **8**, 326-332.
12. H. Uoyama, K. Goushi, K. Shizu, H. Nomura and C. Adachi, *Nature*, 2012, **492**, 234-238.
13. Y. Tao, K. Yuan, T. Chen, P. Xu, H. Li, R. Chen, C. Zheng, L. Zhang and W. Huang, *Adv. Mater.*, 2014, **26**, 7931-7958.
14. J. Lee, K. Shizu, H. Tanaka, H. Nakanotani, T. Yasuda, H. Kaji and C. Adachi, *J. Mater. Chem. C*, 2015, **3**, 2175-2181.
15. K. Meerholz and D. C. Müller, *Adv. Funct. Mater.*, 2001, **11**, 251-253.
16. S. Reineke, F. Lindner, G. Schwartz, N. Seidler, K. Walzer, B. Lüssem and K. Leo, *Nature*, 2009, **459**, 234.
17. S.-Y. Kim, W.-I. Jeong, C. Mayr, Y.-S. Park, K.-H. Kim, J.-H. Lee, C.-K. Moon, W. Brütting and J.-J. Kim, *Adv. Funct. Mater.*, 2013, **23**, 3896-3900.
18. T. Hatakeyama, K. Shiren, K. Nakajima, S. Nomura, S. Nakatsuka, K. Kinoshita, J. Ni, Y. Ono and T. Ikuta, *Adv. Mater.*, 2016, **28**, 2777-2781.
19. W. Zeng, H. Y. Lai, W. K. Lee, M. Jiao, Y. J. Shiu, C. Zhong, S. Gong, T. Zhou, G. Xie, M. Sarma, K. T. Wong, C. C. Wu and C. Yang, *Adv. Mater.*, 2018, **30**, 1704961.
20. C. S. Oh, C.-K. Moon, J. M. Choi, J.-S. Huh, J.-J. Kim and J. Y. Lee, *Org. Electron.*, 2017, **42**, 337-342.
21. P. Rajamalli, N. Senthilkumar, P. Y. Huang, C. C. Ren-Wu, H. W. Lin and C. H. Cheng, *J. Am. Chem. Soc.*, 2017, **139**, 10948-10951.
22. H. Kaji, H. Suzuki, T. Fukushima, K. Shizu, K. Suzuki, S. Kubo, T. Komino, H. Oiwa, F. Suzuki, A. Wakamiya, Y. Murata and C. Adachi, *Nat. Commun.*, 2015, **6**, 8476.

23. W. Zhang, J. Jin, Z. Huang, X. Lv, S. Zhuang and L. Wang, *J. Mater. Chem. C*, 2017, **5**, 4636-4644. View Article Online
DOI: 10.1039/C8TC01419A
24. J. W. Sun, J.-H. Lee, C.-K. Moon, K.-H. Kim, H. Shin and J.-J. Kim, *Adv. Mater.*, 2014, **26**, 5684-5688.
25. T. Komino, Y. Sagara, H. Tanaka, Y. Oki, N. Nakamura, H. Fujimoto and C. Adachi, *Appl. Phys. Lett.*, 2016, **108**, 241106.
26. T.-L. Wu, M.-J. Huang, C.-C. Lin, P.-Y. Huang, T.-Y. Chou, R.-W. Chen-Cheng, H.-W. Lin, R.-S. Liu and C.-H. Cheng, *Nat. Photon.*, 2018, DOI: 10.1038/s41566-018-0112-9.
27. Y. Im, M. Kim, Y. J. Cho, J.-A. Seo, K. S. Yook and J. Y. Lee, *Chem. Mater.*, 2017, **29**, 1946-1963.
28. S. Nowy, B. C. Krummacher, J. Frischeisen, N. A. Reinke and W. Brütting, *J. Appl. Phys.*, 2008, **104**, 123109.
29. D. Yokoyama, *J. Mater. Chem.*, 2011, **21**, 19187-19202.
30. T. Komino, H. Tanaka and C. Adachi, *Chem. Mater.*, 2014, **26**, 3665-3671.
31. T. Komino, Y. Oki and C. Adachi, *Sci. Rep.*, 2017, **7**, 8405.
32. D. Zhang, X. Song, M. Cai, H. Kaji and L. Duan, *Adv. Mater.*, 2018, **30**, 1705406.
33. J.-A. Seo, Y. Im, S. H. Han, C. W. Lee and J. Y. Lee, *ACS Appl. Mat. Interfaces*, 2017, **9**, 37864-37872.
34. A. Endo, K. Sato, K. Yoshimura, T. Kai, A. Kawada, H. Miyazaki and C. Adachi, *Appl. Phys. Lett.*, 2011, **98**, 083302.
35. K. Sato, K. Shizu, K. Yoshimura, A. Kawada, H. Miyazaki and C. Adachi, *Phys. Rev. Lett.*, 2013, **110**, 247401.
36. D. Zhang, L. Duan, C. Li, Y. Li, H. Li, D. Zhang and Y. Qiu, *Adv. Mater.*, 2014, **26**, 5050-5055.
37. S. O. Jeon, T. Earmme and S. A. Jenekhe, *J. Mater. Chem. C*, 2014, **2**, 10129-10137.
38. J. Li, T. Nakagawa, J. MacDonald, Q. Zhang, H. Nomura, H. Miyazaki and C. Adachi, *Adv. Mater.*, 2013, **25**, 3319-3323.
39. T.-A. Lin, T. Chatterjee, W.-L. Tsai, W.-K. Lee, M.-J. Wu, M. Jiao, K.-C. Pan, C.-L. Yi, C.-L. Chung, K.-T. Wong and C.-C. Wu, *Adv. Mater.*, 2016, **28**, 6976-6983.
40. T. Komino, H. Nomura, T. Koyanagi and C. Adachi, *Chem. Mater.*, 2013, **25**, 3038-3047.
41. D. Zhang, X. Song, M. Cai and L. Duan, *Adv. Mater.*, 2018, **30**, 1705250.
42. J. Tan, B. Wang, Z. Huang, X. Lv, W. Yi, S. Zhuang and L. Wang, *J. Mater. Chem. C*, 2016, **4**, 5222-5230.
43. S. Y. Liu, X. G. Chen and C. W. Zhang, *Thin Solid Films*, 2015, **584**, 176-185.
44. G. Honggang, C. Xiuguo, J. Hao, Z. Chuanwei and L. Shiyuan, *J. Opt.*, 2016, **18**, 025702.

The linear and stereoscopic structures were realized in two TADF isomers. With the smaller ΔE_{ST} , better thermal stabilities and preferential horizontal orientation, the device based **IndCzpTr-2** realized EQE_{max} of 30.0%, the blue-green TADF OLED with EQE_{max} of 14.5% was obtained for **IndCzpTr-1** with homologous device structure.

